buildings

Article

Flood Disaster Risk Assessment in Wuhan City Based on GIS Analysis and Indicator Ranking Using Random Forest

Jingrong Wu [1,2,*] and Xiang Jiang [1]

[1] Faculty of Architecture, Civil Engineering and Environment, Hubei University of Technology, Wuhan 430068, China; 102110853@hbut.edu.cn
[2] College of Engineering Technology, Hubei University of Technology, Wuhan 430068, China
* Correspondence: 102110854@hbut.edu.cn

Abstract: In recent years, with the acceleration of urbanization and the frequent occurrence of extreme weather globally, the risk of urban flood disasters has gradually increased, and its potential consequences are immeasurable. Therefore, conducting risk assessment of urban flood disasters is of great significance, as it is one of the foundations and decision-making means for Disaster Prevention and Mitigation, and has become a hot topic and trend in current research. This paper starts by exploring the concept and formation mechanism of urban flood disasters, taking Hazard Factors, Disaster-prone Environment sensitivity, Vulnerability of Exposed Bodies, and Disaster Prevention and Mitigation Capabilities as primary indicators. Based on this, a risk assessment index system is established with 14 secondary indicators, such as annual average rainfall, distance to water systems, elevation, and terrain undulation. The spatialization of each indicator data point is processed through ArcGIS10.7, and the importance of hazard and sensitivity indicators is ranked using the Random Forest algorithm. The indicators are then weighted using a combination of the Analytic Hierarchy Process (AHP) and the entropy method, and the combined weights of each assessment indicator are calculated. Taking Wuhan City as the research area, the weights of each indicator are input into the established risk assessment model. ArcGIS spatial analysis techniques and raster calculation functions are utilized to solve the fuzzy comprehensive evaluation of the assessment model, obtaining zoning maps of risk levels for hazard, sensitivity, vulnerability, disaster prevention, and mitigation capabilities, as well as the distribution of comprehensive risk levels. The validity and rationality of the model results are verified by actual disaster data, providing important reference for urban flood disaster prevention in the future.

Keywords: flood disaster; risk assessment; ArcGIS; random forest; composite weighting

check for updates

Citation: Wu, J.; Jiang, X. Flood Disaster Risk Assessment in Wuhan City Based on GIS Analysis and Indicator Ranking Using Random Forest. *Buildings* **2024**, *14*, 1370. https://doi.org/10.3390/buildings14051370

Academic Editor: Haifeng Liao

Received: 15 April 2024
Revised: 8 May 2024
Accepted: 9 May 2024
Published: 10 May 2024

1. Introduction

Natural disasters, as extremely serious natural phenomena, disrupt ecosystems, lead to socio-economic instability, and directly impact the balance of supply and demand for societal resources [1–5]. Flood disasters are an integral component of natural disasters. Jongman [6] argues that over the past few decades, the losses caused by floods globally have been escalating, making floods the most frequent and destructive type of disaster occurring today. To prevent and mitigate the losses caused by disasters, risk assessment is often employed as a decision-making tool. It is a quantitative method aimed at assessing the potential impact and extent of losses that a risk event might bring. Delalay [7] developed a flood risk assessment model that mapped and quantified population vulnerability in the flood-prone areas of the Sindupalchowk District in Nepal. This model identified areas prone to urban flooding. Quesada [8] conducted an analysis and classification of 82 cities in Costa Rica based on the hazard, sensitivity, and vulnerability to floods. They designed a flood risk index to understand the role of risk-driving factors at the local level. Mokhtari [9] utilized the Analytic Hierarchy Process (AHP) to integrate multi-criteria data, such as slope, river network density, soil type, rainfall, population density, land use type, and drainage system density, to identify and map flood-prone areas in the Cheliff-Ghrib watershed. Abdrabo [10] conducted a study in a coastal city in Egypt, where they developed and assessed a urban flood vulnerability index based on the exposure, susceptibility, and resilience of the city to urban flooding.

The commonly adopted methods for flood risk assessment can generally be classified into the following categories: (1) Historical Disaster Records: Using mathematical and statistical methods, combined with historical disaster records in the area, this approach involves a thorough analysis of the hazard, characteristics, and probability of disaster occurrences to better predict future trends [11]. Its calculation method is relatively simple, but still subject to limitations. Firstly, it requires access to long-term and continuous disaster information. However, during the information collection process, it is challenging to ensure consistency, completeness, and authority of the information, making the statistical results less accurate [12]. Secondly, historical disaster data are typically aggregated over larger scales, such as administrative regions and river basins, which reduces the applicability of historical disaster records within specific areas. Benito discussed risk assessment by studying ancient and historical flood data [13]. Benito [14] discussed risk assessment by studying ancient and historical flood data. (2) The Index System Approach: Starting from the mechanism and conditions of disaster formation, this method selects specific risk indicators and factors in the study area. By processing raw data through mathematical methods, it constructs a comprehensive evaluation index system to assess the level of risk. This approach has a wider application scope, convenient data acquisition, and can reflect the macroscopic characteristics of risk distribution in the area. However, it is subject to subjective judgment, and the selected indicators vary greatly between regions, leading to insufficient accuracy [15]. Cai [16] employed the Analytic Hierarchy Process (AHP) with triangular fuzzy numbers to determine the weights of 11 indicators influencing floods. They conducted an in-depth exploration of the dynamic risk patterns and hotspots of precipitation changes to achieve more accurate results. (3) The Remote Sensing and GIS Integration Approach [17,18]: utilizing satellite remote sensing technology to acquire a series of disaster-related information, including flood extent, frequency, duration, and water body data, and integrating GIS data collection and spatial analysis capabilities to conduct visualized analysis of flood disaster risks.

With the development of artificial intelligence and the arrival of the big data era, statistical learning algorithms can be utilized in conjunction with traditional methods to assess flood risk. Random Forest is a powerful machine learning algorithm commonly used for solving classification and regression problems [19]. This method has been applied to predict disease risk [20], forecast stock market direction [21], land cover classification [22], predict crop yield [23], and more. Based on the above research, the Random Forest algorithm has the potential applicability in assessing urban flood disaster risk. By utilizing the Random Forest algorithm to comprehensively assess various indicators and factors related to flood disasters, it can provide valuable support for urban disaster risk assessment.

This study constructs an urban flood disaster risk assessment model. It spatially processes the data of each assessment indicator using ArcGIS10.7. Additionally, it ranks the importance of hazard and sensitivity indicators using the Random Forest algorithm. It adopts a combined Analytic Hierarchy Process (AHP) and entropy method to weight the indicators, obtaining the composite weights of each assessment indicator. Taking Wuhan City as the research subject, it inputs the weights of each indicator into the established risk assessment model. Then, it conducts fuzzy comprehensive evaluation and draws the disaster risk level zoning map on the ArcGIS platform. Furthermore, it validates the final results based on actual disaster data, demonstrating the scientific rationality of the constructed indicator system. This study provides valuable insights and reference for subsequent urban flood disaster prevention measures.

2. Materials and Methods

2.1. Description of the Study Area

Wuhan is situated in the eastern part of the Jianghan Plain, at the heart of the Yangtze River Basin [24]. It stretches approximately 134 km from east to west and about 155 km from north to south, covering an area of 8569.15 square kilometers. With a permanent population of 13.649 million, it consists of 13 administrative districts. Serving as a vital strategic hub in the rise of central China, Wuhan's administrative divisions are depicted in Figure 1. The Yangtze River flows 145 km within the boundaries of Wuhan, with 60 km flowing through the urban area. The width of the Yangtze river surface ranges from 1000 m to 1200 m, reaching up to 3400 m at its widest point. During periods of abundant rainfall and extreme heavy rain, the water level of the Yangtze River can rise to 27–28 m. Historically, the peak water level of the Yangtze River in the Wuhan section reached 29.73 m in 1954 and 29.43 m in 1998. Within the boundaries of Wuhan, the Yangtze River is joined by tributaries such as Dongjing River, Han River, Fu River, She River, Dao River, and Ju River to the north, and larger tributaries such as Jinshui River, Xunsi River, and Qingshan Port to the south. The Han River and Fu River converge with the Yangtze River within the main urban area of Wuhan. Wuhan city boasts abundant lake resources and is known as the "City of a Hundred Lakes". According to statistics from the Wuhan Lake Bureau, there are a total of 166 lakes within the city's boundaries, with a total water area of 5925.2 square kilometers and a total water surface area of 779 square kilometers under normal water levels. Among them, 40 lakes are distributed within the main urban area of Wuhan.

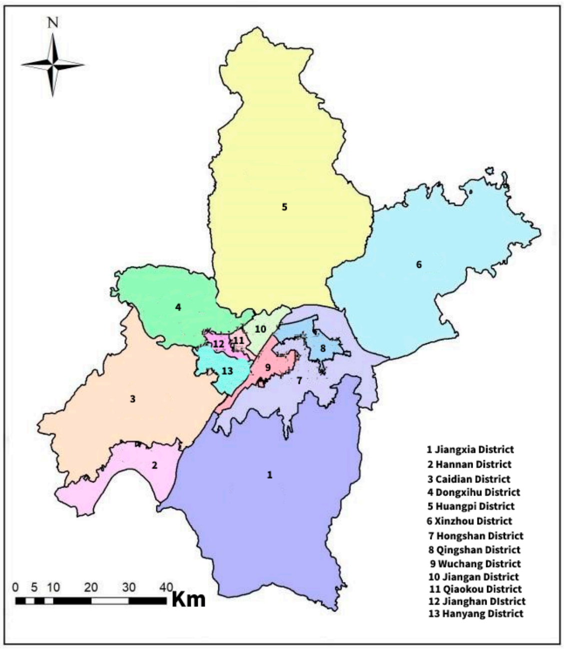

Figure 1. Wuhan administrative district map.

2.2. Assessment System

Based on the principles of selecting evaluation indicators, we construct a risk assessment model for urban flood disasters from four aspects: the Hazard of Causative Factors, Vulnerability of Disaster-prone Environment, Vulnerability of Exposed Bodies, and Disaster Prevention and Mitigation Capability [25–27], we input the data from each indicator layer into ArcGIS for processing to assess the risk of urban flood disasters.

(1) Hazard of Causative Factors [28]. The main causative factor for urban flood disasters is typically heavy rainfall, especially under extreme conditions. Therefore, we use annual average precipitation and distance to water bodies as evaluation indicators to study the Hazard of Causative Factors. Using the spatial analysis module in ArcGIS, we downloaded monthly precipitation data for each district in Wuhan from the Chinese

Academy of Sciences Data Center for the years 2000 to 2020. We filtered and summarized the data in Excel2021 to calculate the total precipitation for each year by summing the monthly values. We divided the total precipitation by the number of years to obtain the annual average precipitation for each district in Wuhan. We saved this vector data and imported it into ArcGIS to join it with the administrative boundaries of Wuhan's districts. We applied kriging interpolation analysis to generate raster data of the annual average precipitation for Wuhan. We downloaded hydrological data for Wuhan from the National Geographical Information Resource Catalog Service System. We imported the data into ArcGIS for Euclidean distance analysis. We established multi-level buffer zones based on the distance from lakes and rivers, categorized into five intervals: <200 m, 200 m~500 m, 500 m~1000 m, 1000 m~3000 m, >3000 m, as shown in Figure 2.

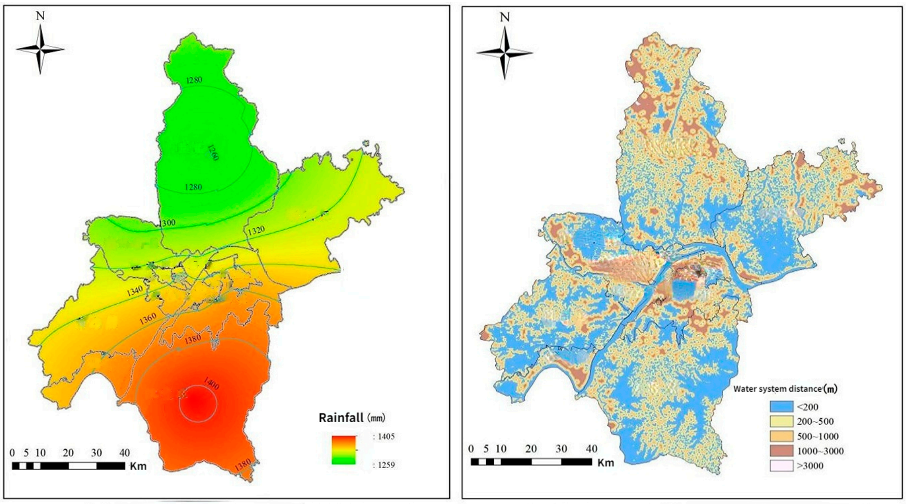

(a) Distribution Map of Average Rainfall in Wuhan City (b) Distribution map of water system distance in Wuhan City

Figure 2. Hazard of Causative Factors.

(2) Vulnerability of Disaster-prone Environment [29]. As the background for flood disaster occurrence, the Disaster-prone Environment typically represents the attributes of the underlying surface. It generally consists of the geographical location, terrain features, natural hydrological conditions, and vegetation coverage of the urban environment. We selected elevation, terrain undulation, slope, river network density, and vegetation coverage area as evaluation indicators. We selected SRTM data provided by NASA with a resolution of 30 m. Import elevation data for Hubei Province and use masking extraction to clip out the elevation data for Wuhan City. Based on the elevation characteristics, we applied the natural breaks classification method in ArcGIS to divide the elevation data for Wuhan City into five different levels, from low to high. When calculating terrain ruggedness, the focal statistics function in ArcGIS 10.7is commonly used to process elevation data. This helps calculate the difference between high and low points within a specified range, resulting in a terrain standard deviation classification map. Using ArcGIS's slope analysis tool, we generated slope information for the Wuhan area based on elevation data. We imported the data downloaded from OpenStreetMap into ArcGIS and clipped it. We used the raster calculator to assign zero values to any null values. We converted the raster data to points and perform kriging interpolation to obtain the distribution of river network density in Wuhan, as shown in Figure 3.

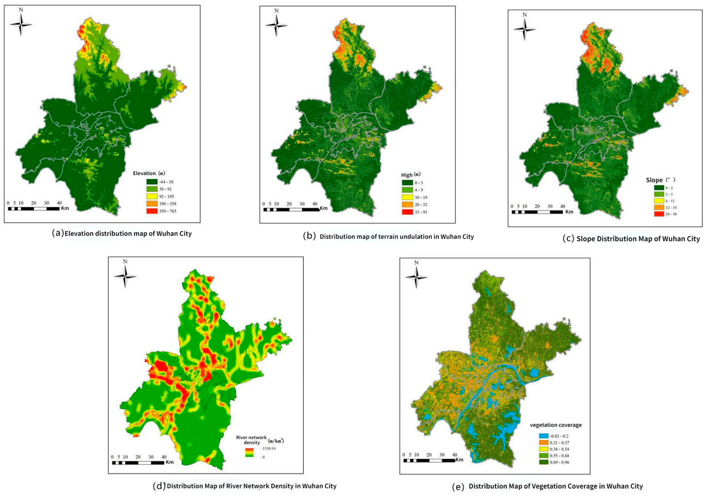

Figure 3. Vulnerability of Disaster-prone Environment.

(3) Vulnerability of Exposed Bodies. Based on human safety and socio-economic factors, if an area has a larger population and more developed economy, the damage caused by flood disasters will be greater [30]. Typically, the vulnerability level of flood disasters is used to describe the severity of this situation. In this paper, the indicators selected for vulnerability assessment are population density, GDP per unit area, and land use types. We selected the data for these indicators with their corresponding units, and performed masking extraction to obtain Figure 4.

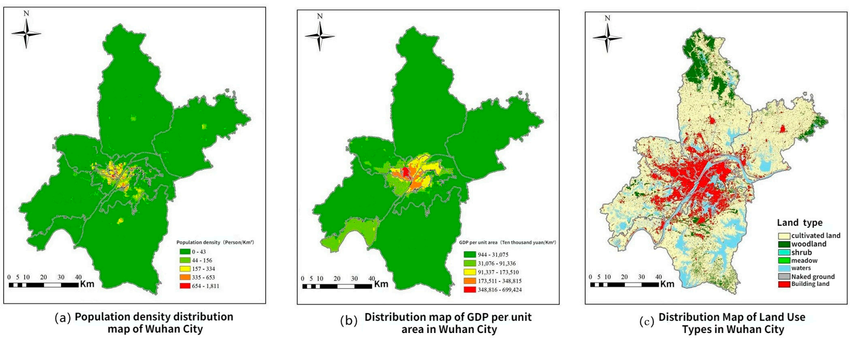

Figure 4. Vulnerability of Exposed Bodies.

(4) Disaster Prevention and Mitigation Capability. This refers to humanity's defense and resistance capabilities in the face of flood disasters. The societal capacity to withstand disasters can reduce the losses caused by disasters [31]. The stronger the capacity, the lower the losses. This paper selects medical rescue capability, road density, and financial support capability to reflect the region's Disaster Prevention and Mitigation Capabilities. We selected the 2020 national point of interest (POI) data and extracted medical service data. We imported and clipped it to obtain relevant medical points of interest in Wuhan City. We utilized the kernel density analysis tool in spatial analysis, employing geometric intervals to classify it into five categories. We downloaded national road data from the OpenStreetMap website, imported it, and clipped it to obtain road data for Wuhan City. We used the raster calculator to assign zero values to any null values. We converted the raster data to points and performed kriging interpolation to obtain road density data for Wuhan City. We downloaded vector data for regional GDP and local fiscal revenue. We calculated per capita GDP by dividing the regional GDP by the population for each region. We imported the data into ArcGIS and rasterized it based on county administrative units. We utilized the standard deviation method for classification to obtain distribution maps for local fiscal revenue and per capita GDP, as shown in Figure 5.

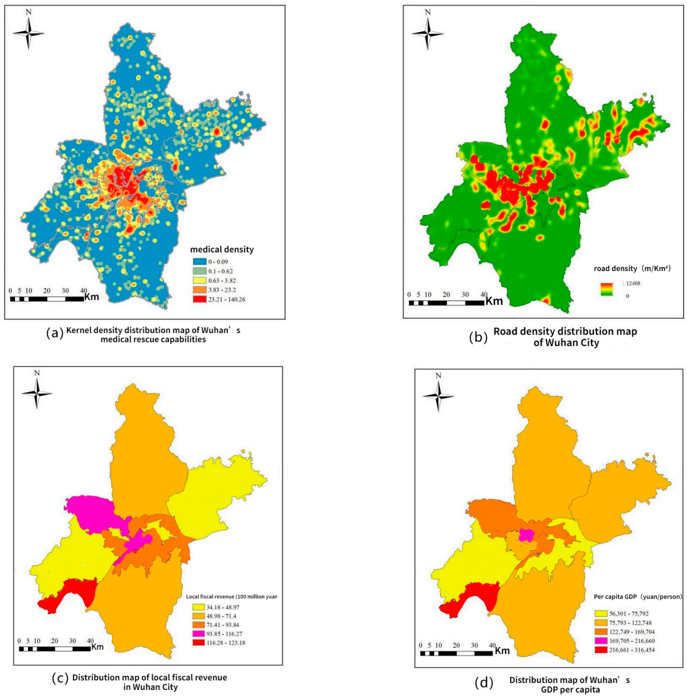

Figure 5. Disaster Prevention and Mitigation Capability.

2.3. Data Source

The risk assessment framework for flood disasters consists of the objective layer, criteria layer, and indicator layer, which are multi-level and composed of complex elements. The sources of each data are presented in Table 1.

Table 1. Data source.

Target Layer	Criterion Layer	Indicator Layer	Data Source
Flood disaster risk assessment	Hazard of Causative Factors [32]	Rainfall	Resources and Environmental Science Data Center
		Water system distance	Resources and Environmental Science Data Center
	Vulnerability of Disaster-prone Environment [33]	Elevation	NASA's Land Processes DAAC
		terrain relief	NASA's Land Processes DAAC
		slope	NASA's Land Processes DAAC
		Vegetation coverage	Resources and Environmental Science Data Center
		River network density	Open Street Map
	Vulnerability of Exposed Bodies	Population density	WorldPop [34]
		GDP	Resources and Environmental Science Data Center
		Land type	Resources and Environmental Science Data Center [35]
	Disaster Prevention and Mitigation Capability	Medical rescue capability	Resources and Environmental Science Data Center
		Road density	Open Street Map
		Local fiscal revenue	Wuhan Bureau of Statistics
		Per capita GDP	Wuhan Bureau of Statistics

2.4. Random Forest Analysis

Through Random Forest analysis, we can evaluate the influence of feature factors on the final results. The risk factors are set as feature vectors (X), and the flood points (extracted from the 2020 Wuhan flood disaster data and inundation maps) were set as target vectors (Y) [36–38]. Since flood disasters are only related to pre-disaster environmental factors, and the rescue capabilities of various regions after the disaster cannot be reflected by flood disasters, Random Forest classification analysis was conducted on pre-disaster environmental factors such as hazard and sensitivity indicators.

When optimizing the number of decision trees, n_estimators refers to the number of sub-datasets generated by bootstrap sampling with replacement from the original dataset, which is the number of decision trees. If it is too small, it may lead to model underfitting, and if it is too large, it may reduce the significance of the model. The parameter range is chosen to be 20 to 400. max_features refers to the maximum number of features considered when building the optimal model of the decision tree, generally ranging from 2 to 10, while the remaining parameters are set to default values. The accuracy of the algorithm is detected through ten-fold cross-validation, and the dataset is divided into training and testing sets, with 90% and 10%, respectively. The GridSearchCV tool in sklearn is used on the training set to find the parameters with the highest accuracy.

Parameter adjustment is continuously verified, and it is found that when n_estimators = 118 and max_features = 5, the accuracy is 0.93706. As shown in Figures 6 and 7, the cross-validation set is repeatedly modified until the highest accuracy of 0.94418 is obtained.

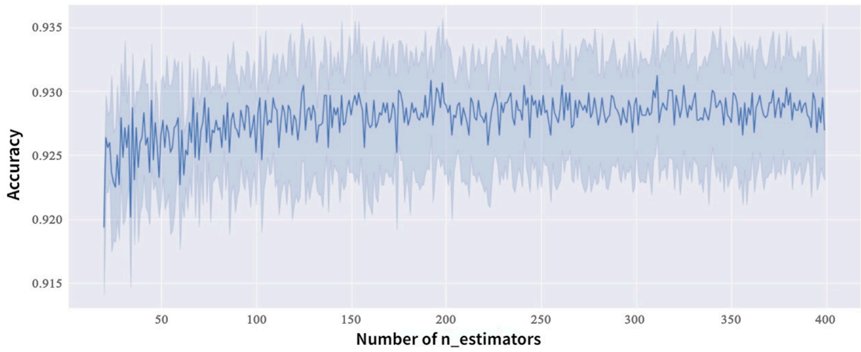

Figure 6. The highest accuracy of n_estimators.

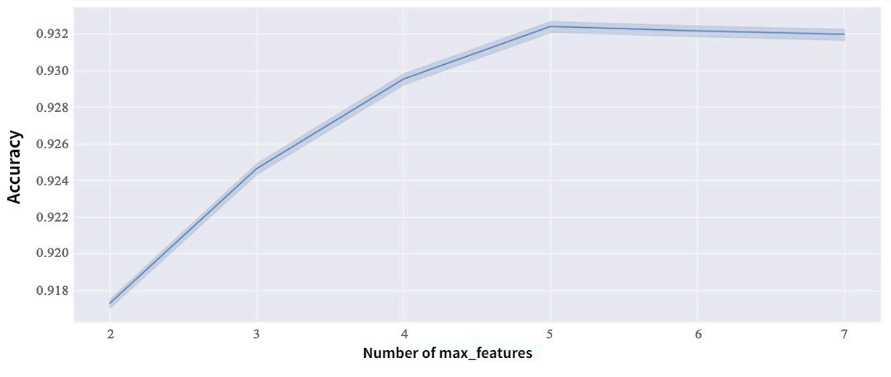

Figure 7. The highest accuracy of max_features.

In the hazard indicator of flood risk, the proportion of annual average rainfall is the highest, indicating the highest importance level, reaching 41.8%. Following that are vegetation coverage, elevation, and river network density, accounting for 16.1%, 12.1%, and 12.0%, respectively. They also show strong correlations. In comparison, slope, terrain undulation, and distance to water bodies have the lowest importance levels in the impact of urban flood disasters, at 7.7%, 5.4%, and 4.9%, respectively, indicating a relatively minor impact on disasters, as shown in Figure 8.

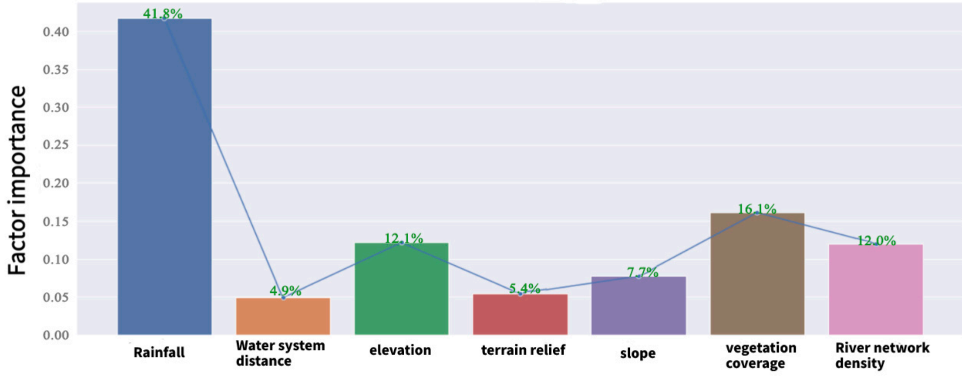

Figure 8. Importance ranking.

2.5. Subjective Weight Calculation

By using the Analytic Hierarchy Process (AHP) to calculate the subjective weights [39], we construct judgment matrices based on the importance of various indicators obtained from the Random Forest [40,41]. According to the expert scoring method, we determine the importance of each indicator. Through the established evaluation model, judgment matrices are created for each primary and secondary indicator, and all judgment matrices pass consistency checks, ensuring that indicators at each level are reasonably allocated. Finally, we integrate and rank the indicators and calculate the weights of each level, obtaining the subjective comprehensive weight distribution of the 14 indicators, as shown in Tables 2–7.

Table 2. The allocation of weights for primary indicators.

Evaluation Indicators	Hazard	Sensitivity	Vulnerability	Disaster Prevention and Mitigation Capability	Weight
Hazard	1	2	2	3	0.4236
Sensitivity	1/2	1	1	2	0.2270
Vulnerability	1/2	1	1	2	0.2270
Disaster Prevention and Mitigation Capability	1/3	1/2	1/2	1	0.1223

$\lambda max = 4.0104$, CI = 0.0035, CR = 0.0039 < 1.

Table 3. Allocation of weights for hazard indicators.

Evaluation Indicators	Rainfall	Water System Distance	Weight
Rainfall	1	2	0.6667
Water system distance	1/2	1	0.3333

$\lambda max = 2.000$, CI = 0.0000, CR = 0.0000 < 1.

Table 4. Allocation of weights for sensitivity indicators.

Evaluation Indicators	Elevation	Terrain Relief	Slope	River Network Density	Vegetation Coverage	Weight
Elevation	1	2	2	3	4	0.2392
Terrain relief	1/2	1	1	3	4	0.1079
Slope	1/2	1	1	3	3	0.1079
River network density	1/3	1/3	1/3	1	3	0.1801
Vegetation coverage	1/4	1/4	1/3	1/3	1	0.3649

$\lambda max = 5.0719$, CI = 0.0180, CR = 0.0161 < 1.

Table 5. Allocation of weights for vulnerability indicators.

Evaluation Indicators	Population Density	GDP	Land Type	Weight
Population density	1	3	4	0.6144
GDP	1/3	1	3	0.2648
land type	1/4	1/3	1	0.1172

λmax = 3.0735, CI = 0.0368, CR = 0.0707 < 1.

Table 6. Allocation of weights for Disaster Prevention and Mitigation Capability indicators.

Evaluation Indicators	Medical Rescue Capability	Per Capita GDP	Local Fiscal Revenue	Road Density	Weight
Medical rescue capability	1	2	3	4	0.2392
Per capita GDP	1/2	1	3	4	0.1079
Local fiscal revenue	1/2	1	3	3	0.1079
Road density	1/3	1/3	1	3	0.1801

λmax = 4.1596, CI = 0.0532, CR = 0.0598 < 1.

Table 7. Comprehensive weight allocation.

Evaluation Indicators	Hazard	Sensitivity	Vulnerability	Disaster Prevention and Mitigation Capability	Subjective Comprehensive Weight
Rainfall	0.8000	–	–	–	0.3389
Water system distance	0.2000	–	–	–	0.0847
Elevation	–	0.2392	–	–	0.0543
Terrain relief	–	0.1079	–	–	0.0245
Slope	–	0.1079	–	–	0.0245
River network density	–	0.1801	–	–	0.0409
vegetation coverage	–	0.3649	–	–	0.0829
Population density	–	–	0.6144	–	0.1395
GDP	–	–	0.2684	–	0.0609
Land type	–	–	0.1172	–	0.0266
Medical rescue capability	–	–	–	0.2254	0.0276
Per capita GDP	–	–	–	0.5023	0.0614
Local fiscal revenue	–	–	–	0.0942	0.0115
Road density	–	–	–	0.1781	0.0218

2.6. Objective Weight Calculation

From an objective weight calculation using the entropy method, the results obtained show strong objective factors [42,43]. Through analyzing the differences in raster values of flood disaster indicators, it can be inferred that the greater the data difference under the same indicator, the higher the information entropy, thus increasing the comparative importance of the indicator in risk assessment and leading to a higher weight value. In this paper, after preprocessing the multi-source data of flood indicators and using normalization calculation methods based on the classification characteristics of positive and negative indicators, the objective weight values of flood indicators at all levels are finally obtained. Please refer to Table 8 for details.

Table 8. Objective weight allocation.

Evaluation Indicators	Hazard	Sensitivity	Vulnerability	Disaster Prevention and Mitigation Capability
Rainfall	0.0339	–	–	–
Water system distance	0.0111	–	–	–
Elevation	–	0.0007	–	–
Terrain relief	–	0.0010	–	–
Slope	–	0.0017	–	–
River network density	–	0.1615	–	–

Table 8. *Cont.*

Evaluation Indicators	Hazard	Sensitivity	Vulnerability	Disaster Prevention and Mitigation Capability
Vegetation coverage	–	0.0502	–	–
Population density	–	–	0.4090	–
GDP	–	–	0.2655	–
Land type	–	–	0.0368	–
Medical rescue capability	–	–	–	0.0004
Per capita GDP	–	–	–	0.0085
Local fiscal revenue	–	–	–	0.0186
Road density	–	–	–	0.0012

2.7. Combination Weighting Calculation

We determined the subjective and objective weights of each evaluation indicator using Analytic Hierarchy Process (AHP) and entropy method, respectively, and calculated the comprehensive weight based on the differences between the two weighting methods for each indicator. Finally, we obtained the comprehensive weight through the distance function of both methods.

The distance function expression between subjective weights and objective weights is given by [44]:

$$d(W_{ai}, W_{si}) = \left[\frac{1}{2}\sum_{i=1}^{m}(W_{ai} - W_{si})^2\right]^{\frac{1}{2}}, \tag{1}$$

The difference between α and β represents the difference between allocation coefficients:

$$D = |\alpha - \beta|, \tag{2}$$

According to the previous text, the constructed equation for calculating the comprehensive weight is:

$$\begin{cases} \frac{1}{2}\sum_{i=1}^{m} (W_{ai} - W_{si})^2 = (\alpha - \beta)^2 \\ (\alpha + \beta) = 1 \end{cases}, \tag{3}$$

The expression for the combination weight is given by:

$$W_i = \alpha W_{ai} + \beta W_{si}, \tag{4}$$

W_{ai} is the subjective weight, W_{si} is the objective weigh, α, β are the allocation coefficients for the weights.

The final calculation yields the combination weights of flood risk assessment indicators. The combination weighting results are shown in Table 9.

Table 9. Combined weighting.

Evaluation Indicators	Hazard	Sensitivity	Vulnerability	Disaster Prevention and Mitigation Capability
Rainfall	0.1864	–	–	–
Water system distance	0.0479	–	–	–
Elevation	–	0.0275	–	–
Terrain relief	–	0.0127	–	–
Slope	–	0.0131	–	–
River network density	–	0.1012	–	–
Vegetation coverage	–	0.0666	–	–
Population density	–	–	0.2742	–
GDP	–	–	0.1632	–
Land type	–	–	0.0317	–
Medical rescue capability	–	–	–	0.0140

Table 9. *Cont.*

Evaluation Indicators	Hazard	Sensitivity	Vulnerability	Disaster Prevention and Mitigation Capability
Per capita GDP	–	–	–	0.0350
Local fiscal revenue	–	–	–	0.0150
Road density	–	–	–	0.0115

2.8. Constructing the Membership Function

The membership function essentially reflects the objective research object, and the degree of membership, as the foundation, can describe the fuzziness of factors [45]. Through the membership function, fuzzy evaluation methods can be applied to solve practical problems [46,47]. In this paper, fuzzy distribution combination is mainly used to construct the membership function to evaluate flood risk in Wuhan City. The construction method is as follows: first, the evaluation indicator data is divided into different levels, and the most commonly used ascending and descending trapezoidal functions and triangular functions are selected. The descending trapezoidal function is used for the low-value area, while the ascending trapezoidal function is used for the high-value part. The middle value part is represented by a triangular function. This construction of membership functions is more in line with actual situations, as shown in Figure 9.

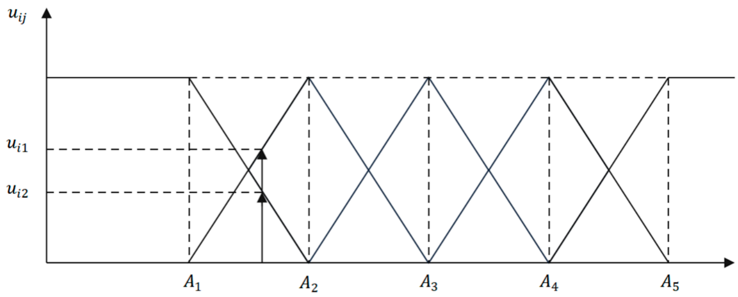

Figure 9. Membership function for risk assessment.

The results of flood risk assessment are intricately linked to the classification of raster data for each evaluation indicator [48]. Based on the different research data, this paper adopts the principle of maximum membership degree to determine the membership degree of each raster cell. Through map algebra functions, the membership degree values corresponding to five levels for each raster cell of individual indicators in the study area can be obtained. Then, based on the determined combination weights, the layers of hazard, sensitivity, vulnerability, Disaster Prevention and Mitigation Capability, and comprehensive evaluation are calculated. Finally, the risk index is determined by the principle of maximum membership degree to obtain the risk level of each raster cell. The classification of indicator data in this paper is shown in Table 10.

Table 10. Table of indicator data classification.

Evaluation Indicators	A1	A2	A3	A4	A5
Rainfall (mm)	1291	1317	1342	1372	1406
Water system distance (m)	205	505	900	1501	3479
Elevation (m)	38	91	195	358	785
Terrain relief (m)	3	9	19	32	91
Slope (°)	2	5	11	19	50
River network density (m/km^2)	108	294	492	780	1531
Vegetation coverage	0.2	0.37	0.54	0.68	0.96
Population density (Person/km^2)	43	156	334	653	1811

Table 10. *Cont.*

Evaluation Indicators	A1	A2	A3	A4	A5
GDP (Ten thousand yuan/km^2)	31,075	91,336	173,510	348,815	699,424
Medical rescue capability	0.09	0.62	3.82	23.2	140.26
Road density (m/km^2)	487	1577	3163	5936	12,408
Per capita GDP (yuan/Person)	75,792	122,748	169,704	216,660	316,454
Local fiscal revenue (billion yuan)	48.97	71.40	93.84	116.27	123.18

3. Results

3.1. Fuzzy Comprehensive Evaluation of Flood Risk in Wuhan City

According to the calculation results of the combination weights, the disaster indicator weights are combined with the raster cell data to obtain the disaster risk assessment results for Wuhan City. The formula for the flood risk assessment model is as follows [49]:

$$DRI = W_1 \times H + W_2 \times E + W_3 \times V + W_4 \times R, \quad (5)$$

DRI is the risk degree; W_1, W_2, W_3, W_4 are the combination weights of hazard H, sensitivity E, vulnerability V, and resilience R, respectively.

Low risk, slightly less risk, medium risk, slightly higher risk, and high risk correspond with risk index ranges as follows: DRI < 0.35, 0.35 < DRI < 0.45, 0.45 < DRI < 0.60, 0.60 < DRI < 0.70, DRI > 0.70.

3.2. Hazard Assessment

As one of the four criteria layers, hazard severity has a significant impact on the assessment of flood risk. According to the flood risk assessment model, the hazard severity of flooding in Wuhan is illustrated in Figure 10.

From the figure, it can be observed that the central and southern regions of Wuhan have higher hazard severity, while areas of lower severity are mainly distributed in the northern low hills. There is a gradient increase in hazard severity from north to south. Specifically, large portions of Jiangxia District exhibit high hazard severity, as well as some areas in Hongshan District, Hannan District, and Caidian District. These areas have numerous water systems and lakes, and they typically experience abundant rainfall throughout the year. Similarly, central urban districts such as Wuchang, Hankou, Jianghan, Jiang'an, and Qiaokou also demonstrate relatively high hazard severity due to their high level of urbanization. The Huangpi District has the lowest hazard severity.

Utilizing ArcGIS, the areas and percentages of different levels of flood hazard severity in Wuhan were calculated. As shown in Table 11, the proportion of high hazard severity areas is the largest at 29.24%, while low hazard severity areas comprise the smallest proportion at 7.44%.

Table 11. Areas and percentages of different risk levels.

Risk Levels	Area (km^2)	Percentage of Total City Area
High risk	2511.17	29.24%
Slightly higher risk	2349.83	27.38%
Medium risk	1972.06	22.98%
Slightly less risk	1112.18	12.96%
Low risk	638.20	7.44%

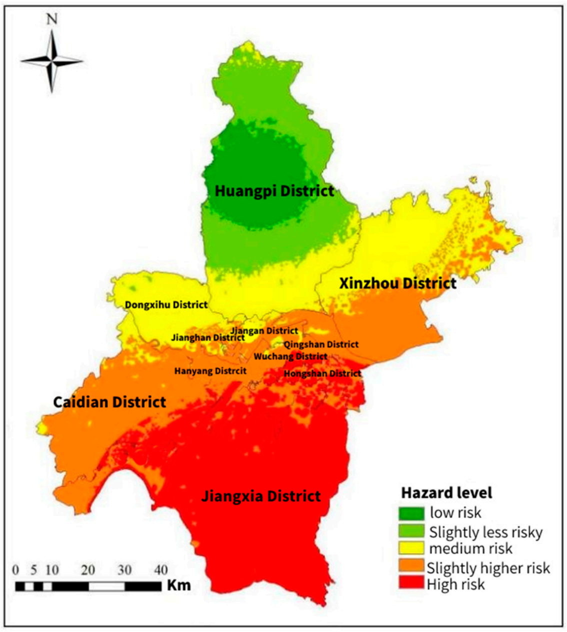

Figure 10. Map of flood risk levels distribution in Wuhan City.

3.3. Sensitivity Assessment

The flood hazard reflects the sensitivity of the study area to high-intensity rainfall events, considering factors such as topography, vegetation, and river networks. In this study, the sensitivity of Wuhan City to flooding was assessed based on the analysis of elevation, terrain undulation, slope gradient, river network density, and vegetation coverage, as shown in Figure 11.

From the distribution in the figure, it is evident that there is a strong correlation between sensitivity and the actual development of the city. Areas with high sensitivity are mostly concentrated in the central part of the city, particularly along the western bank of the Yangtze River. The main reason for this is that these areas are located in the plains, with relatively gentle terrain and low vegetation coverage. The high concentration of buildings and high level of urbanization increase the risk of urban flooding. Examples include districts such as Hanyang, Jianghan, Hankou, Jiang'an, Qiaokou, Hannan, and Dongxihu. Additionally, certain areas in Wuchang and Hongshan districts also exhibit high sensitivity to flooding.

Furthermore, some parts of the Huangpi and Xinzhou Districts show elevated sensitivity, forming bands of high-risk areas. This is attributed to the presence of rivers traversing the area, leading to a higher river network density and increased flood sensitivity. In contrast, Jiangxia and Caidian districts exhibit the lowest sensitivity. These areas have higher vegetation coverage and are situated in hilly terrain, resulting in some surface undulation and slope gradient. This facilitates rapid runoff and infiltration of precipitation, thereby reducing the sensitivity to flooding risks.

Based on the raster data, the statistical calculation of the proportion of different levels of flood sensitivity areas in Wuhan City is presented in Table 12, showing the areas and their corresponding percentages. The proportions of low sensitivity and relatively low sensitivity represent the extremes, accounting for 38.81% and 4.55%, respectively.

Table 12. Areas and percentages of different sensitivity levels.

Sensitivity Levels	Area (km^2)	Percentage of Total City Area
High sensitivity	1641.37	19.16%
Slightly higher sensitivity	2085.39	24.35%
Medium sensitivity	1124.05	13.12%
Slightly less sensitivity	389.87	4.55%
Low sensitivity	3324.04	38.81%

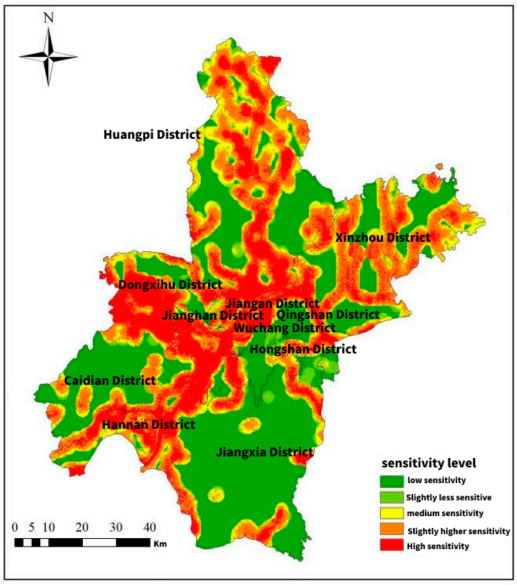

Figure 11. Distribution map of sensitivity levels to flood disasters in Wuhan City.

3.4. Vulnerability Assessment

The vulnerability assessment of flood hazards in Wuhan City focuses on population density, per capita GDP, and land use type data. By integrating these indicators with their respective composite weights, the vulnerability to flood hazards in Wuhan is evaluated. The results are depicted in Figure 12.

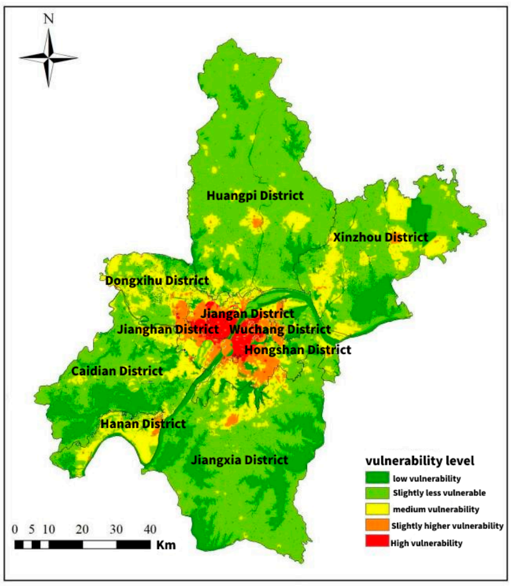

Figure 12. Distribution of vulnerability levels of flood hazards in Wuhan City.

Overall, the distribution of vulnerability to urban flood hazards in Wuhan City exhibits a gradual decrease from the city center to the surrounding areas. High vulnerability areas are mostly concentrated in districts such as Wuchang, Qiaokou, Jianghan, and Jiang'an. These areas have higher population density, predominantly urban land use, with agricultural land as secondary, and superior socioeconomic conditions compared to the rest of the city. Consequently, these areas exhibit the highest vulnerability to similar levels of disaster. Additionally, districts like Hankou, Hongshan, and Qingshan also show relatively high vulnerability due to their relatively advanced socioeconomic status, despite not having as concentrated a population as the main urban areas. However, as the population density, economic development level, and urbanization gradually decrease from the city center to the outskirts, areas with moderate, lower, and low vulnerability are formed. Both the northern and southern parts of the city exhibit lower vulnerability and less land development, such as in Huangpi, Xinzhou, and most areas of Jiangxia belonging to low vulnerability zones. According to grid data, the statistical analysis of vulnerability risk level areas and their proportions in Wuhan City are shown in Table 13. Overall, most areas of Wuhan City have low vulnerability, with higher vulnerability proportions mainly concentrated in the central urban areas.

Table 13. Areas and percentages of different vulnerability levels.

Vulnerability Levels	Area (km^2)	Percentage of Total City Area
High vulnerability	136.14	1.59%
Slightly higher vulnerability	328.43	3.83%
Medium vulnerability	1396.60	16.28%
Slightly less vulnerability	5083.82	59.25%
Low vulnerability	1635.93	19.06%

3.5. Disaster Prevention and Reduction Capabilities Assessment

The Disaster Prevention and Mitigation Capabilities reflect both societal and individual resilience in facing the onslaught of heavy rain and flood disasters. Strong Disaster Prevention and Mitigation Capabilities are associated with lower risk coefficients of flood disasters. Key data include medical rescue capabilities, local financial revenue, per capita GDP, and road density. By spatializing these indicator data, computing fuzzy membership degrees, and integrating the combination weights of each indicator, an assessment of the Disaster Prevention and mitigation Capabilities is conducted using the raster calculation function in ArcGIS, as shown in Figure 13.

Areas with moderate to high Disaster Prevention and Mitigation Capabilities in Wuhan are concentrated in regions such as Hannan District, Dongxihu District, Jiang'an District, and Wuchang District. These areas have experienced rapid economic development, high per capita GDP, advanced medical standards, and dense road networks. Residents and local governments are capable of conducting emergency rescue operations promptly, thus exhibiting relatively high capabilities in preventing and responding to heavy rain and flood disasters. Conversely, areas with lower Disaster Prevention and Mitigation Capabilities include Huangpi District, Xinzhou District, Jiangxia District, Qingshan District, Hongshan District, and Caidian District. This is mainly influenced by local economic development and medical standards. Based on raster data calculations, the final distribution of areas and their respective proportions are summarized in Table 14. Overall, Wuhan's Disaster Prevention and Mitigation Capabilities against flood disasters are generally low, indicating a need for strengthening efforts to resist and prevent disasters.

Table 14. Area and percentage of different levels of disaster prevention and mitigation capabilities.

Disaster Prevention and Reduction Capabilities Levels	Area (km^2)	Percentage of Total City Area
High	275.09	3.20%
Slightly higher	2.89	0.03%
Medium	680.87	7.93%
Slightly less	3694.39	43.04%
Low	3930.24	45.79%

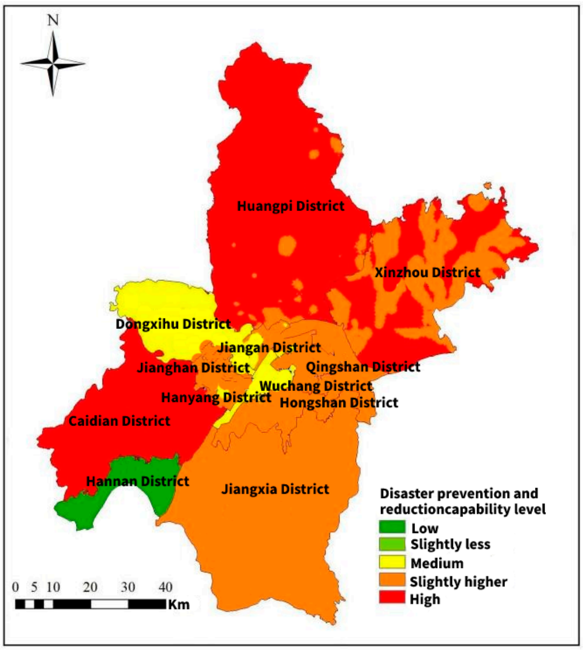

Figure 13. Disaster Prevention and Mitigation Capability level distribution map of flood disasters in Wuhan City.

4. Discussion

When the risk factors of flood disasters, including their hazards, environmental sensitivity to disaster occurrence, and vulnerability of exposed populations, are higher, the flood risk in that area is greater. Conversely, stronger Disaster Prevention and Mitigation Capabilities in a region lead to lower flood risk. By assigning comprehensive weights and conducting flood risk assessment calculations, the final evaluation results are obtained, as shown in Figure 14.

From the graph, it can be observed that the high-risk areas for flood disasters in Wuhan mainly concentrate in the central urban area, particularly on the west bank of the Yangtze River, where the situation is quite severe. Specifically, Jianghan District, Qiaokou District, Jiang'an District, and Wuchang District are most affected. Additionally, parts of Dongxihu District, Qingshan District, Hongshan District, and Hankou District belong to areas with relatively high flood risks, resulting in an overall moderate-to-moderately-high flood risk level. Huangpi District, Xinzhou District, and Caidian District generally have lower flood risks, but there are still some areas within them with medium-to-high risks. Areas around Hannan and Jiangxia are mostly low-risk zones.

Looking at the distribution, Wuhan's flood risk presents a pattern of high risk in the central areas and low risk at the periphery. In the central urban area, due to the flat terrain, low elevation, proximity to water bodies, low vegetation coverage, and a high proportion of impermeable surfaces, flood risks are elevated. Additionally, the dense population in these areas would lead to incalculable losses in the event of flood disasters. Huangpi District and Xinzhou District have abundant vegetation and higher elevations, categorizing them as areas with lower-to-moderate flood risks. However, flood risks in the central part of the Hongshan District are relatively dispersed, with many scattered areas of medium-to-high flood risks, especially in areas adjacent to Wuchang, where urban development is significant, population density is high, vegetation is sparse, and large impermeable surface areas exist, resulting in elevated flood risks. The Dongxihu District generally falls into the moderate flood risk category, despite its dense river network, due to a lower urban population density, higher per capita GDP, higher local fiscal revenue, and greater road density compared to the central urban area, leading to slightly lower flood risks. Low-risk areas are mainly distributed in Jiangxia District and Hannan District. Some areas in Jiangxia have higher elevations and good vegetation coverage, coupled with a lower urban population density and a larger proportion of water bodies, leading to lower potential disaster losses. Hannan is still in the process of development and construction, hence currently poses the lowest risk among these two regions.

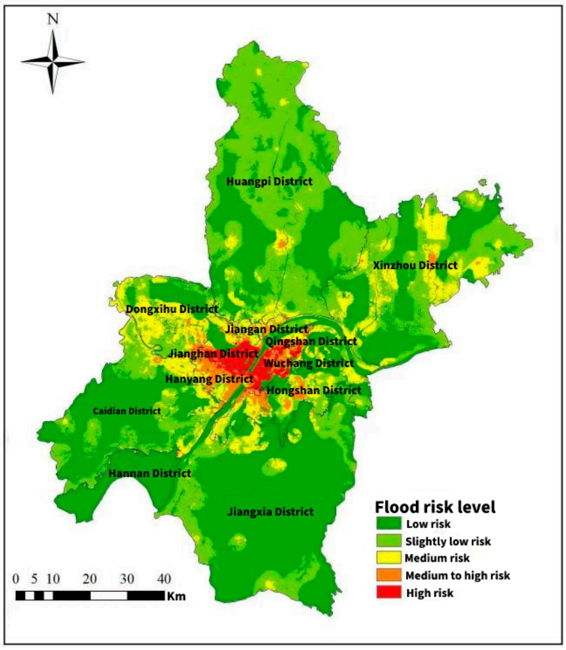

Figure 14. Comprehensive risk level distribution map of flood disasters in Wuhan.

By conducting area statistics calculations, the proportions of different flood risk levels in Wuhan are shown in Table 15. The area proportion of low-risk zones is the highest, accounting for 49.63%, followed by moderately low-risk zones at 34.76%. High-risk areas have the lowest area proportion, merely 1.28%, while moderate- and moderately-high-risk zones account for 11.62% and 2.71%, respectively.

Table 15. Area and percentage of flood risk at different levels in Wuhan.

Risk Levels	Area (km^2)	Percentage of Total City Area
High risk	109.60	1.28%
Slightly higher risk	232.28	2.71%
Medium risk	995.15	11.62%
Slightly less risky	2976.75	34.76%
Low risk	4250.94	49.63%

In order to ensure the credibility and accuracy of disaster data, the flood risk data from the updated 2020 version of the inundation risk map released by the Wuhan Water Affairs Bureau were utilized. Each vulnerable point in the map corresponds to a specific coordinate system. Using ArcGIS spatial processing, the data were overlaid onto the flood risk assessment map of Wuhan City for disaster inspection. The results are shown in Figure 15.

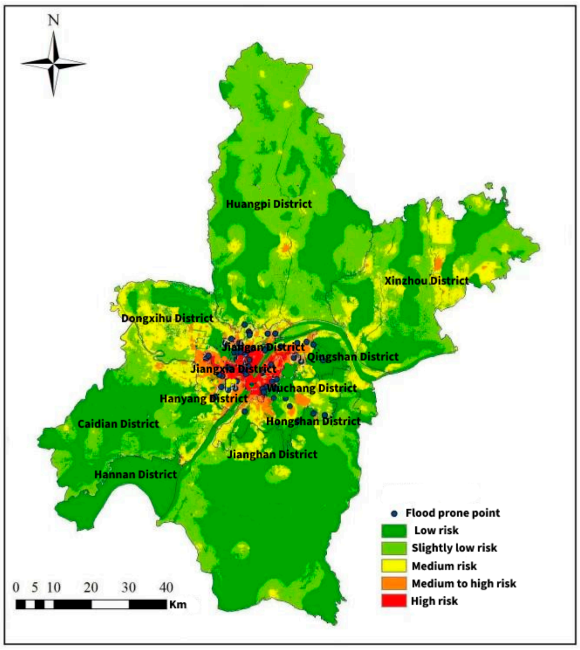

Figure 15. Comparison and verification map of waterlogging prone points and risk zoning results in Wuhan.

Analysis of the results from the graph reveals that the distribution of vulnerable points aligns closely with the final distribution of disaster risk depicted in the map. Vulnerable points are predominantly concentrated in the central urban areas, such as around the Jianghan District, Qiaokou District, Jiang'an District, and Wuchang District. By comparing the inundation-prone points within Wuhan with the final results of disaster risk distribution, although the sample size for disaster validation is limited, it can be concluded that the flood risk assessment results obtained in this study are generally consistent with historical disaster situations, indicating a relatively high level of accuracy.

5. Conclusions

1. Using the Random Forest algorithm, it was determined that, among the factors contributing to flood risk and vulnerability to disaster in the city, the annual average rainfall index had the highest importance, accounting for 41.8%. Following this, vegetation coverage, elevation, and river network density were identified as significant factors, accounting for 16.1%, 12.1%, and 12.0%, respectively. Slope, terrain ruggedness, and distance to water bodies were found to have the lowest importance in urban flood disaster impact, accounting for 7.7%, 5.4%, and 4.9%, respectively.
2. Based on the results obtained from the Random Forest algorithm, the final weights were calculated using a combination weighting method. Among these weights, the highest weight was assigned to the annual average rainfall, which was 0.1864. Conversely, the lowest weight was assigned to road density, with a value of 0.0115.
3. The concentration of inundation-prone points in Wuhan City is primarily in the areas around the Jianghan District, Jiangan, and Wuchang Districts. The high degree of alignment between the flood risk assessment map of Wuhan City and the 2020 updated inundation risk map indicates a high level of accuracy in the urban flood disaster risk assessment model constructed in this study.

Author Contributions: Conceptualization, J.W. and X.J.; methodology, J.W.; software, X.J.; validation, X.J.; formal analysis, J.W. and X.J.; data curation, X.J.; writing—original draft preparation, X.J.;

writing—review and editing, J.W. and X.J.; supervision, J.W. All authors have read and agreed to the published version of the manuscript.

Funding: This research was funded by the National Natural Science Foundation of China General Project (grant number: 42071264); Program of Hubei Province Construction Science and Technology Plan (grant number: 2021082).

Data Availability Statement: The data presented in this study are available on request from the corresponding author.

Conflicts of Interest: All authors declare that the research was conducted in the absence of any commercial or financial relationships that could be construed as a potential conflicts of interest.

References

1. Bhavnani, R. *Natural Disaster Conflicts*; Harvard University: Cambridge, MA, USA, 2006.
2. Kokai, M.; Fujii, S.; Shinfuku, N.; Edwards, G. Natural disaster and mental health in Asia. *Psychiatry Clin. Neurosci.* **2004**, *58*, 110–116. [CrossRef] [PubMed]
3. Neumayer, E.; Plümper, T.; Barthel, F. The political economy of natural disaster damage. *Glob. Environ. Chang.* **2014**, *24*, 8–19. [CrossRef]
4. Sawada, Y.; Takasaki, Y. Natural disaster, poverty, and development: An introduction. *World Dev.* **2017**, *94*, 2–15. [CrossRef]
5. Yu, M.; Yang, C.; Li, Y. Big data in natural disaster management: A review. *Geosciences* **2018**, *8*, 165. [CrossRef]
6. Jongman, B.; Winsemius, H.C.; Aerts, J.C.; Coughlan de Perez, E.; Van Aalst, M.K.; Kron, W.; Ward, P.J. Declining vulnerability to river floods and the global benefits of adaptation. *Proc. Natl. Acad. Sci. USA* **2015**, *112*, E2271–E2280. [CrossRef] [PubMed]
7. Delalay, M.; Ziegler, A.D.; Shrestha, M.S.; Wasson, R.J.; Sudmeier-Rieux, K.; McAdoo, B.G.; Kochhar, I. Towards improved flood disaster governance in Nepal: A case study in Sindhupalchok District. *Int. J. Disaster Risk Reduct.* **2018**, *31*, 354–366. [CrossRef]
8. Quesada-Román, A. Flood risk index development at the municipal level in Costa Rica: A methodological framework. *Environ. Sci. Policy* **2022**, *133*, 98–106. [CrossRef]
9. Mokhtari, E.; Mezali, F.; Abdelkebir, B.; Engel, B. Flood risk assessment using analytical hierarchy process: A case study from the Cheliff-Ghrib watershed, Algeria. *J. Water Clim. Chang.* **2023**, *14*, 694–711. [CrossRef]
10. Abdrabo, K.I.; Kantoush, S.A.; Esmaiel, A.; Saber, M.; Sumi, T.; Almamari, M.; Elboshy, B.; Ghoniem, S. An integrated indicator-based approach for constructing an urban flood vulnerability index as an urban decision-making tool using the PCA and AHP techniques: A case study of Alexandria, Egypt. *Urban Clim.* **2023**, *48*, 101426. [CrossRef]
11. Van Bavel, B.; Curtis, D. Better understanding disasters by better using history: Systematically using the historical record as one way to advance research into disasters. *Int. J. Mass Emergencies Disasters* **2016**, *34*, 143–169. [CrossRef]
12. Dominey-Howes, D. Documentary and geological records of tsunamis in the Aegean Sea region of Greece and their potential value to risk assessment and disaster management. *Nat. Hazards* **2002**, *25*, 195–224. [CrossRef]
13. Aryal, K.R. The history of disaster incidents and impacts in Nepal 1900–2005. *Int. J. Disaster Risk Sci.* **2012**, *3*, 147–154. [CrossRef]
14. Benito, G.; Ouarda, T.; Bárdossy, A. Applications of palaeoflood hydrology and historical data in flood risk analysis. *J. Hydrol.* **2005**, *313*, 1–2. [CrossRef]
15. Cardona, O.D. Indicators of disaster risk and risk management. *IDRiM J.* **2011**, *1*, 27–47. [CrossRef]
16. Cai, S.; Fan, J.; Yang, W. Flooding risk assessment and analysis based on GIS and the TFN-AHP method: A case study of Chongqing, China. *Atmosphere* **2021**, *12*, 623. [CrossRef]
17. Gao, J. Integration of GPS with remote sensing and GIS: Reality and prospect. *Photogramm. Eng. Remote Sens.* **2002**, *68*, 447–454.
18. Weng, Q. Modeling urban growth effects on surface runoff with the integration of remote sensing and GIS. *Environ. Manag.* **2001**, *28*, 737–748. [CrossRef] [PubMed]
19. Biau, G. Analysis of a random forests model. *J. Mach. Learn. Res.* **2012**, *13*, 1063–1095.
20. Khalilia, M.; Chakraborty, S.; Popescu, M. Predicting disease risks from highly imbalanced data using random forest. *BMC Med. Inform. Decis. Mak.* **2011**, *11*, 51. [CrossRef]
21. Khaidem, L.; Saha, S.; Dey, S.R. Predicting the direction of stock market prices using random forest. *arXiv* **2016**, arXiv:1605.00003.
22. Hayes, M.M.; Miller, S.N.; Murphy, M.A. High-resolution landcover classification using Random Forest. *Remote Sens. Lett.* **2014**, *5*, 112–121. [CrossRef]
23. Everingham, Y.; Sexton, J.; Skocaj, D.; Inman-Bamber, G. Accurate prediction of sugarcane yield using a random forest algorithm. *Agron. Sustain. Dev.* **2016**, *36*, 27. [CrossRef]
24. Han, S.S.; Wu, X. Wuhan. *Cities* **2004**, *21*, 349–362. [CrossRef]
25. Arduino, G.; Reggiani, P.; Todini, E. Recent advances in flood forecasting and flood risk assessment. *Hydrol. Earth Syst. Sci.* **2005**, *9*, 280–284. [CrossRef]
26. Lyu, H.-M.; Shen, S.-L.; Zhou, A.; Yang, J. Perspectives for flood risk assessment and management for mega-city metro system. *Tunn. Undergr. Space Technol.* **2019**, *84*, 31–44. [CrossRef]
27. Tsakiris, G. Flood risk assessment: Concepts, modelling, applications. *Nat. Hazards Earth Syst. Sci.* **2014**, *14*, 1361–1369. [CrossRef]

28. Wahba, M.; Hassan, H.S.; Elsadek, W.M.; Kanae, S.; Sharaan, M. Novel utilization of simulated runoff as causative parameter to predict the hazard of flash floods. *Environ. Earth Sci.* **2023**, *82*, 333. [CrossRef]
29. Shano, L.; Raghuvanshi, T.K.; Meten, M. Landslide susceptibility evaluation and hazard zonation techniques—A review. *Geoenviron. Disasters* **2020**, *7*, 18. [CrossRef]
30. Karmakar, S.; Simonovic, S.P.; Peck, A.; Black, J. An information system for risk-vulnerability assessment to flood. *J. Geogr. Inf. Syst.* **2010**, *2*, 129. [CrossRef]
31. Yang, L.; Cao, C.; Wu, D.; Qiu, H.; Lu, M.; Liu, L. Study on typhoon disaster loss and risk prediction and benefit assessment of disaster prevention and mitigation. *Trop. Cyclone Res. Rev.* **2018**, *7*, 237–246.
32. Xie, Y.D.; Jiang, C.K. Dataset of frequency distribution parameters of annual precipitation in China. *Resour. Environ. Sci. Data Regist. Publ. Syst.* **2022**. [CrossRef]
33. Kobrick, M.; Crippen, R. *NASA Shuttle Radar Topography Mission Global 30 arc Second*; NASA EOSDIS Land Processes Distributed Active Archive Center: Sioux Falls, SD, USA, 2024; Available online: https://doi.org/10.5067/MEaSUREs/SRTM/SRTMGL30.002 (accessed on 7 May 2024).
34. WorldPop. The Spatail Distribution of Population Density in 2020, China. 2020. Available online: https://doi.org/10.5258/SOTON/WP00674 (accessed on 8 February 2024).
35. Xu, X.L. Dataset of spatial distribution of multi-temporal ecosystem types in China. *Resour. Environ. Sci. Data Regist. Publ. Syst.* **2023**. [CrossRef]
36. Schoppa, L.; Disse, M.; Bachmair, S. Evaluating the performance of random forest for large-scale flood discharge simulation. *J. Hydrol.* **2020**, *590*, 125531. [CrossRef]
37. Wang, Z.; Lai, C.; Chen, X.; Yang, B.; Zhao, S.; Bai, X. Flood hazard risk assessment model based on random forest. *J. Hydrol.* **2015**, *527*, 1130–1141. [CrossRef]
38. Zhu, Z.; Zhang, Y. Flood disaster risk assessment based on random forest algorithm. *Neural Comput. Appl.* **2022**, *34*, 3443–3455. [CrossRef]
39. Lawal, D.U.; Yusof, K.W.; Hashim, M.A.; Balogun, A.-L. Spatial analytic hierarchy process model for flood forecasting: An integrated approach. In *Proceedings of the IOP Conference Series: Earth and Environmental Science*; IOP Publishing: Bristol, UK, 2014; p. 012029.
40. Chen, Y.-R.; Yeh, C.-H.; Yu, B. Integrated application of the analytic hierarchy process and the geographic information system for flood risk assessment and flood plain management in Taiwan. *Nat. Hazards* **2011**, *59*, 1261–1276. [CrossRef]
41. Stefanidis, S.; Stathis, D. Assessment of flood hazard based on natural and anthropogenic factors using analytic hierarchy process (AHP). *Nat. Hazards* **2013**, *68*, 569–585. [CrossRef]
42. Malekinezhad, H.; Sepehri, M.; Pham, Q.B.; Hosseini, S.Z.; Meshram, S.G.; Vojtek, M.; Vojteková, J. Application of entropy weighting method for urban flood hazard mapping. *Acta Geophys.* **2021**, *69*, 841–854. [CrossRef]
43. Sepehri, M.; Malekinezhad, H.; Hosseini, S.Z.; Ildoromi, A.R. Assessment of flood hazard mapping in urban areas using entropy weighting method: A case study in Hamadan city, Iran. *Acta Geophys.* **2019**, *67*, 1435–1449. [CrossRef]
44. Lai, C.; Chen, X.; Chen, X.; Wang, Z.; Wu, X.; Zhao, S. A fuzzy comprehensive evaluation model for flood risk based on the combination weight of game theory. *Nat. Hazards* **2015**, *77*, 1243–1259. [CrossRef]
45. Civanlar, M.R.; Trussell, H.J. Constructing membership functions using statistical data. *Fuzzy Sets Syst.* **1986**, *18*, 1–13. [CrossRef]
46. Dombi, J. Membership function as an evaluation. *Fuzzy Sets Syst.* **1990**, *35*, 1–21. [CrossRef]
47. Turksen, I. Measurement of membership functions and their acquisition. *Fuzzy Sets Syst.* **1991**, *40*, 5–38. [CrossRef]
48. Liong, S.Y.; Lim, W.H.; Kojiri, T.; Hori, T. Advance flood forecasting for flood stricken Bangladesh with a fuzzy reasoning method. *Hydrol. Process.* **2000**, *14*, 431–448. [CrossRef]
49. Zhao, J.; Jin, J.; Xu, J.; Guo, Q.; Hang, Q.; Chen, Y. Risk assessment of flood disaster and forewarning model at different spatial-temporal scales. *Theor. Appl. Climatol.* **2018**, *132*, 791–808. [CrossRef]